AXISYMMETRIC AND ASYMMETRIC BEHAVIORS
OF A RED BLOOD CELL IN CAPILLARIES

Ting Ye and Hua Li

School of Mechanical and Aerospace Engineering, Nanyang Technological University, 50 Nanyang Avenue
Singapore 639798, Republic of Singapore

Keywords: Red blood cell, Membrane force, Tank treading, Capillary flow, Computational biomechanics.

Abstract: The axisymmetric and asymmetric behaviours of a red blood cell (RBC) in capillaries are investigated numerically by developing a two-fluid model, in which the membrane force is considered to describe the RBC deformation. The quantitative validations with the experimental and theoretical results are provided, and good agreements are found in the deformation index and deformed RBC shapes. The present results show that the RBC experiences the axisymmetric motion if the membrane force is balanced between the RBC cusps, otherwise the asymmetric motion occurs. The characteristic parachute shape of deformed RBC is observed in the axisymmetric motion, while the tank-treading motion of RBC membrane is generated in the asymmetric motion. As the capillary diameter increases, the decrease in RBC length is accompanied by an increase in RBC width.

1 INTRODUCTION

Red blood cells (RBCs) play an essential role in delivering oxygen to the body tissues via blood flow through capillaries in all vertebrates and some invertebrates. In human, a healthy mature RBC is biconcave disk 8 μm in diameter and 2 μm in thickness, which consists of cytoplasm enclosed by a thin membrane (Evans and Fung, 1972). The RBC membrane can experience stretching and bending deformations subject to the blood flow, thereby it is mainly responsible for the mechanical and rheological behaviours of the RBC. It is well known that RBCs are involved in many diseases, such as the sickle-cell anemia resulted from the RBC abnormality, and the capillary blockage due to the RBC fragments. Therefore, it is of great importance to study the behaviours of a RBC in capillaries for revealing the mechanism of RBC deformation and providing the insight into the RBC fighting against relevant diseases.

Generally, a RBC in a capillary experiences an axisymmetric motion, where the RBC is axisymmetric with respect to the central axis of the capillary due to the very small diameter (Secomb, 1987). In this motion, the RBC gradually deforms from a biconcave shape into a parachute one. This parachute shape is the characteristics of a RBC in a

capillary, which guarantes the RBC traversing through various capillaries successfully, including the smaller capillaries compared with the undeformed RBC. The previously published works (Secomb, 1987, Tsukada *et al.*, 2001, Jeong *et al.*, 2006, Tomaiuolo *et al.*, 2009) demonstrate that the deformability of RBC in capillaries depends on the RBC velocity and capillary diameter largely. With increasing the RBC velocity or decreasing the capillary diameter, the RBC width becomes narrower accompanied by an increase of the length. Thus, even though the capillary is very narrow, the RBC may be squeezed through it successfully. Instead of an individual RBC, Pozrikidis (2005) numerically analyzed the axisymmetric motion of a file of RBCs through capillaries using a boundary integral method, and also examined the effects of the cell spacing and capillary radius. However, if the capillary diameter is quite large, the RBC shape cannot be assumed to be axisymmetric any more with respect to the central axis of the capillary. As a result, the RBC will undergo an asymmetric motion. Secomb and Skalak (1982) studied the asymmetric motion of a RBC in a two-dimensional capillary based on the lubrication method. They pointed out that the tank-treading motion of the RBC membrane usually accompies this motion. In other words, the RBC membrane always rotates around the

cytoplasm in the asymmetric motion, like the tank treading. In order to understand the tank-treading motion, Sugihara-Seki and Skalak (1988) investigated the asymmetric flow of a file and two files RBCs using the finite element method, in which each RBC is assumed as a rigid cylinder post and not located at the centerline of capillary. Although a certain progress has been achieved so far, the detailed knowledge of the flow behaviors of a RBC in capillaries is still of interest, especially for the asymmetric motion of RBC.

In the present work, a two-fluid system is developed to model the flow characteristics of a RBC in capillaries, in which the mechanical behavior of the RBC membrane is taken into consideration. Subsequently, validations of this system are carried out by comparing with the experimental and theoretical results. Finally, the axisymmetric behaviors of a RBC in capillaries are simulated systematically on the basis of the two-fluid system. Apart from that, the asymmetric motion of the RBC in the capillary is also analyzed in detailed, as well as the effect of the capillary diameter.
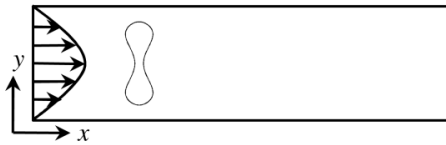
2 MODELS AND METHODS

Figure 1: 2D schematic diagram of a RBC in a capillary subject to the plasma flow with parabolic velocity profile.

The 2D schematic diagram of a RBC in a capillary is provided in Figure 1, in which a plasma flow with a parabolic velocity profile passes through the capillary along the x direction. The 2D RBC with zero velocity is put in the plasma flow, whose shape is expressed as the parametric form (Evans and Fung, 1972),

$$\begin{cases} x = x_0 + r\cos\theta(c_0 + c_1\sin^2\theta + c_2\sin^4\theta), \\ y = y_0 + r\sin\theta, \end{cases} \quad (1)$$

where (x_0, y_0) is the RBC centre, r the maximum radius, and θ the polar angular in the range $[0, 2\pi]$. The three coefficients c_0, c_1 and c_2 are usually taken as 0.1035, 1.0013 and −0.5614, respectively. Due to the stress of the plasma flow, the RBC will move and deform.

2.1 Governing Equations

A two-fluid system is developed here to describe the fluid states of the RBC and plasma. The material properties of fluids inside and outside the RBC are different, such as density and viscosity. By treating these two fluids as a single fluid with variable material properties, the incompressible Navier-Stokes equations are used over the whole domain to describe the motion of the single fluid, written as

$$\begin{cases} \nabla \cdot \boldsymbol{u} = 0, \\ \dfrac{\partial \rho \boldsymbol{u}}{\partial t} + \nabla \cdot (\rho \boldsymbol{u}\boldsymbol{u}) = -\nabla p + \nabla \cdot [\mu(\nabla \boldsymbol{u} + \nabla \boldsymbol{u}^T)] + \boldsymbol{F}, \end{cases} \quad (2)$$

where $\boldsymbol{u}$ is the velocity vector, ρ and μ are the density and viscosity of fluid, t is the time, p is the pressure. The membrane force $\boldsymbol{F}$ reflects the interaction between the RBC and plasma as the result of the membrane deformation, given by

$$\boldsymbol{F} = \int_{\Gamma(t)} \boldsymbol{f}(s,t)\delta(\boldsymbol{x} - \boldsymbol{x}_m)ds, \quad (3)$$

where $\boldsymbol{x}$ and $\boldsymbol{x}_m$ are the spatial variable and membrane position of $\Gamma(t)$, s is the membrane length, $\delta(\boldsymbol{x})$ is the 2D Dirac delta function, and $\boldsymbol{f}(s, t)$ is the membrane force strength.

The membrane force strength can be derived by the shell model (Pozrikdis, 2003), in which the membrane is treated as a thin shell with finite thickness, allowed to undergo bending and stretching deformations, expressed by

$$\boldsymbol{f}(s,t) = \left(\frac{d\tau}{ds} + \kappa\frac{dm}{ds}\right)\boldsymbol{t} + \left(\frac{d^2m}{ds^2} - \kappa\tau\right)\boldsymbol{n}, \quad (4)$$

where τ and m are the in-plane tension and bending moment, $\boldsymbol{t}$ and $\boldsymbol{n}$ are the unit tangent and normal vectors, and κ is the curvature of the membrane. Introducing the constitutive equations, the in-plane tension and bending moment are expressed as

$$\tau = E_s\varepsilon \text{ and } m = E_B(\kappa - \kappa_0), \quad (5)$$

where E_S and E_B are the shear modulus and bending stiffness, ε is the membrane strain, and κ_0 the resting curvature of the membrane.

2.2 Numerical Methods

In numerical simulations, the computational domain is discretized first by the staggered grid system. Based on this grid system, the governing equations are divided into three parts to be solved, namely

calculating the membrane force, tracking the membrane and solving the Navier-Stokes equations.

In order to calculate the membrane force, the membrane is discretized by a set of Lagrangian particles. Any two neighbouring Lagrangian particles are connected by a straight line as a membrane element. Thus, the strain and curvature of each membrane element are obtained easily, followed by the membrane force strength in Eq. (4) by the finite difference method. Figure 2 shows comparisons of the membrane force strength at a fixed state between the numerical and exact results, in which good agreement is observed. After that, Eq. (3) is approximated by the trapezoidal rule so that the calculation of the membrane force is completed.
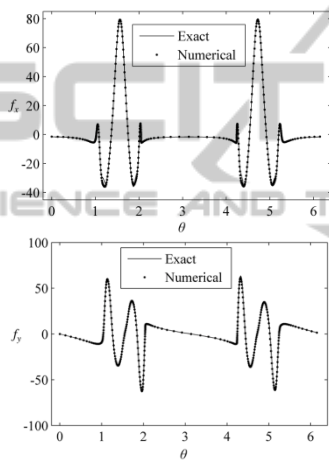

Figure 2: Comparisons of the membrane force strength between the numerical and exact results. The top (*a*) and bottom (*b*) figures correspond to the non-dimensional *x*- and *y*-components of membrane force strength, respectively.

The material properties inside and outside RBC are different, such that the membrane needs tracking to distinguish the RBC and plasma. Besides, the membrane position should be provided for calculating the membrane force by Eq. (3). For these two purposes, the binary level set method (Lie *et al*., 2006) is used to track the membrane, in which a binary level set function is defined to distinguish the plasma and RBC, and governed by a convection function. By solving the convection function using the WENO scheme (Shu, 1997), the membrane can be tracked. However, the accuracy of tracking the membrane is not good due to the numerical dissipation. In order to overcome the disadvantage, the Lagrangian particles scattered to calculate the membrane force are used again to correct the binary level set function.

Finally, a hybrid method coupled SIMPLER (Patankar, 1981) and SIMPLEC (Van-Doormaal and Raithby, 1984) is developed to solve the Navier-Stokes equations, after the material properties of fluid are updated. In this method, a relative accurate pressure field is obtained first by the SIMPLER idea as the initial iterative pressure, and then the velocity field is computed according to the momentum equations. Generally, this velocity field cannot satisfy the continuity equation with the sufficient accuracy. Hence, a velocity correction is provided by the SIMPLEC idea as the second step, which is derived by the continuity equation. These two steps are repeated as an iterative process until both the continuity and momentum equations converge. Thus, the pressure and velocity fields are updated at the current time step.

3 RESULTS AND DISCUSSION

3.1 Validation

In this section, the model is validated by comparing the present numerical predictions with the previously published experiment (Jeong *et al*., 2006, Tomaiuolo *et al*., 2009) and theoretical (Secomb, 1987) results.
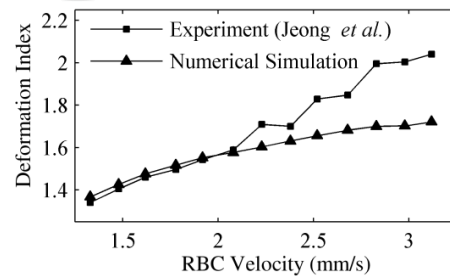

Figure 3: Comparison of the predicted deformation index with the experimental result (Jeong *et al*., 2006).

Jeong *et al*. (2006) investigated experimentally the RBC deformation in the rat mesenteric capillaries. In their work, the effects of the diameter and length of capillary are examined, as well as the RBC velocity on the deformation index, defined as the ratio of the length to diameter of the deformed RBC (Tsukada *et al.* 2001). Here, we focus on one of them, the relationship between the deformation index and the velocity of RBC in a capillary with the diameter of 6.2 μm. The comparison between the present numerical and experimental results is shown in Figure 3, in which a good agreement is found in the increasing trend of deformation index. The

average deformation index of RBC in the capillary is about 1.58 very closed to the value of 1.55 reported by Jeong *et al.* (2006). However, the deformation index is smaller than that of Jeong *et al.* (2006) at the higher velocity, which can be explained that the deformed RBC in the experiment is no longer axisymmetric at the higher velocity.

Furthermore, a comparison of the RBC shape at the steady state is illustrated in Figure 4, in which the experimental (Tomaiuolo *et al.*, 2009) and theoretical (Secomb, 1987) shapes are obtained in the capillaries with diameters of 6.6 and 6.0 µm, respectively. As expected, a good agreement is provided in the deformed shapes, although there exist slight differences resulted from the different capillary diameter.
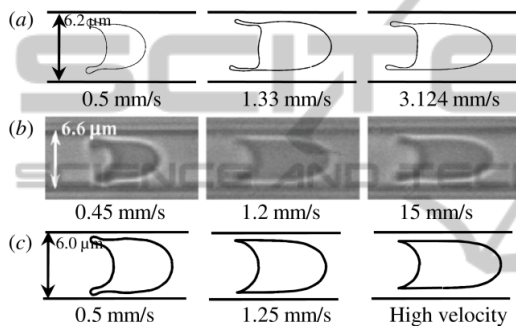

Figure 4: Comparison of the predicted RBC shape (*a*) with the experimental (*b*) (Tomaiuolo *et al.*, 2009) and theoretical results (*c*) (Secomb, 1987).

3.2 Axisymmetric Motion of RBC

When the RBC shape is axisymmetric with respect to the central axis of capillary, it will experience the axisymmetric motion. Figure 5 shows the RBC deformation behaviours in a capillary with the diameter of 10 µm subjected to the maximum flow velocity of 1.25 mm/s. At the initial state, a biconcave RBC is located at the central axis of capillary. In the presence of parabolic blood flow, the RBC deforms gradually to a steady parachute shape, convex in front (at leading surface) and concave at the rear. Meanwhile, the RBC is transported forward, and the RBC shape is always axisymmetric.
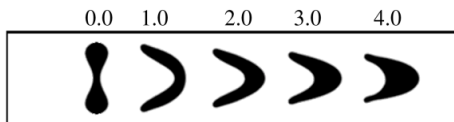

Figure 5: RBC shapes in a capillary at different time, where the number on the top of each snapshot indicates the non-dimensional time *t*.

The axisymmetric deformation behaviour is attributed to the distribution of membrane force strength, as shown in Figure 6. With increasing time, the membrane force strength increases at the sharp cusps and the leading surface, such that the deformation at these parts also becomes larger and larger. At the leading surface the membrane force is generated mainly by the stretching deformation, which makes the RBC outward bulge at the leading surface. However, it is attributed to the bending deformation largely at the sharp cusps, squeezing the sharp cusps narrower and narrower continuously. As a result, the RBC deforms to a steady parachute shape from the initial biconcave shape.
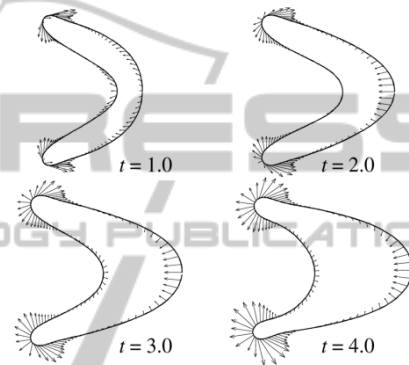

Figure 6: Distribution of membrane force strength at different time, where the number on the bottom right of each snapshot indicates the non-dimensional time.
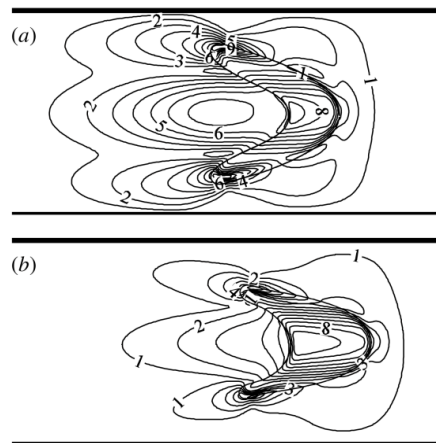

Figure 7: Distribution of the non-dimensional flow speed for a RBC in the capillary. The top (*a*) and bottom (*b*) figures correspond to the non-dimensional time of 2.0 and 4.0, respectively.

Figure 7 illustrates the contour plots of non-dimensional flow speed in ten levels from 0.0 to 0.25. It is found that the flow speed inside the RBC is larger than that in the carrier fluid, such that the

RBC becomes rounder and rounder. Furthermore, the flow speed inside the RBC decreases with increasing time. Once the flow speeds inside and outside the RBC maintain equally each other, the RBC will achieve a steady state.

3.3 Asymmetric Motion of RBC

Apart from the axisymmetric motion, the RBC also undergoes an asymmetric motion if the RBC shape is not axisymmetric with respect to the central axis of the capillary. In this section, the asymmetric motion of the RBC is investigated by locating the RBC near the central axis of the capillary.

Figure 8 depicts the motion and deformation of the RBC, whose centre is placed above and below the central axis of the capillary at the initial state. The leading surface of RBC bulges gradually, while the rear becomes more concave to maintain the area conservation. In addition, the RBC tilts anticlockwise when the RBC centre at the initial state is above the central axis, as shown in Figure 8(*a*). However, the opposite tilt orientation is observed if the RBC centre is below the central axis, as illustrated in Figure 8(*b*). The tilt behaviours are resulted from the parabolic distribution of the flow velocity, which makes the upper and lower parts of RBC undergo the unbalanced velocities. As the RBC tilts gradually, the RBC membrane also rotates around the RBC interior continuously, as found by the motion of the representative node (hollow circle) in Figure 8. This phenomenon is well known as the tank-treading motion of the membrane.
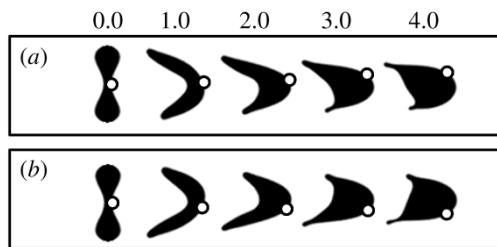

Figure 8: The asymmetric motion of a RBC in the capillary, where the top (*a*) and bottom (*b*) rows are obtained by adjusting the RBC centre slightly above and below the central axis of capillary at the initial state, and the hollow circles refer to the motion of a fixed representative node.

Figure 9 illustrates the distribution of membrane force strength at the non-dimensional time of 3.0 for the RBC centre above and below the central axis of the capillary. It is found that the membrane force strength is significantly large at the sharp cusps. The sharper the cusp is, the larger the membrane force

strength is. This is because that the bending moment plays a dominant role in the membrane part with the large curvature. For example, the curvature at the lower cusp is larger than that at the upper cusp of each deformed RBC in Figure 9. Hence, the membrane force strength is also larger at the lower cusp. The unbalanced membrane force strength at the upper and lower cusps is one of the characteristics of the RBC asymmetric motion, which is different from the RBC axisymmetric motion.
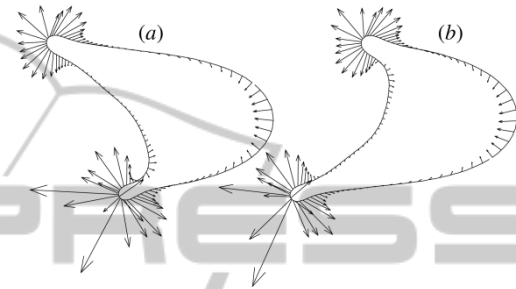

Figure 9: Distribution of the membrane force strength at the non-dimensional time of 3.0 for the RBC centre above (*a*) and below (*b*) the central axis of the capillary.

3.4 Effect of Capillary Diameter

In general, capillary diameter is about 6-10 μm, which has a significant effect on the RBC deformation except the RBC velocity. In this section, the effect of capillary diameter is examined by simulating the motion and deformation of a RBC in the capillaries with diameters of 6.2, 8.0, 10 and 12 μm, respectively. With consideration of the diameter of biconcave RBC, an elliptical RBC with the same area of the biconcave RBC is treated as the initial shape in the capillary of 6.2 μm.
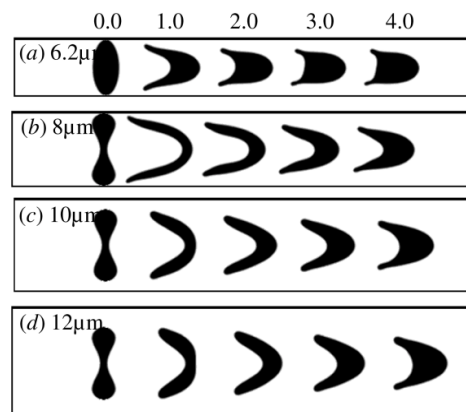

Figure 10: RBC shapes in the capillaries with the different diameter at the different time. The numbers on the top of figure indicate the non-dimensional time.

Figure 10 shows the motion and deformation of a RBC in the different capillaries. As the capillary diameter decreases, the increase in RBC length is accompanied by a decrease in RBC width. Consequently, the deformation index increases with decreasing the capillary diameter. In other words, the RBC has to be elongated more when it passes through a smaller capillary, thereby leading to the increasing trend of the deformation index. This increasing behaviour is attributed to the shear stress of the fluid flow. At a given flow velocity, the shear stress increases with decreasing the capillary diameter, such that the RBC is stretched more obviously at the smaller capillary. In addition, the RBC in the large capillary moves further than that in the small capillary, as indicated in Figure 10(*b*), (*c*) and (*d*). This is because that the RBC is more centralized on the central axis of the capillary when the capillary diameter is larger. At the end, the RBC shape deforms asymmetrically in a small capillary as shown in Figure 10 (a), especially at the non-dimensional time of 4.0. The reason for the asymmetric behaviour is that the shear stress acting on the RBC membrane is more unbalanced if the RBC is closer to the capillary wall, which was also reported by Jeong *et al*. (2006).

4 CONCLUSIONS

The present work concerns a numerical investigation of the axisymmetric and symmetric motion of a RBC in capillaries by developing a two-fluid system. In order to describe the RBC deformation, the membrane force is treated as a singular force coupled into the two-fluid system. A quantitative comparison with the experimental data is carried out by examining the relationship between the deformation index and the RBC velocity, yielding a good agreement. Apart from that, the predicted RBC shapes in the present work are compared with the experimental and theoretical results published, which also reasonably shows good agreements.

The axisymmetric behaviours of a RBC in the capillary are simulated first, in which the characteristic parachute shape is observed. By analyzing the membrane force strength, it is found that the RBC experiences an axisymmetric motion if the membrane force is balanced between the upper and lower cusp of the RBC. Then, the asymmetric behaviours of a RBC are investigated by adjusting the initial position of the RBC in the capillary, in which the tank-treading motion of the RBC membrane is reproduced and the membrane force

strength is not balanced any more. Finally, the effect of the capillary diameter on the RBC deformation is evaluated, where a decrease in RBC length accompanied by an increase in RBC width is observed with increasing the capillary diameter.

ACKNOWLEDGEMENTS

REFERENCES

Evans E., Fung Y., 1972. Improved measurements of the erythrocyte geometry. *Microvasc. Res.,* 4, 335-347.

Jeong J. H., Sugii Y., Minamiyama M., Okamoto K., 2006. Measurement of RBC deformation and velocity in capillaries in vivo. *Microvasc. Res.,* 71, 212-217.

Lie J., Lysaker M., Tai X., 2006. A binary level set model and some applications to Mumford-Shah image segmentation. *IEEE Trans. Image Processing,* 15, 1171-1181.

Patankar S. V., 1981. A calculation procedure for two-dimensional elliptic situations. *Numer Heat Transfer,* 4, 409-425.

Pozrikdis C., 2003. *Modeling and Simulation of Capsules and Biological Cells*, Chapman & Hall/CRC.

Pozrikidis C., 2005. Axisymmetric motion of a file of red blood cells through capillaries. *Phys. Fluids,* 17, 031503.

Secomb T. W., 1987. Flow-dependent rheological properties of blood in capillaries. *Microvasc. Res.,* 34, 46-58.

Secomb T. W., Skalak R., 1982. A two-dimensional model for capillary flow of an asymmetric cell. *Microvasc. Res.,* 24, 194-203.

Shu C., 1997. Essentially non-oscillatory and weighted essentially non-oscillatory schemes for hyperbolic conversation laws. *NASA/CR-97-206253*, ICASE Report No. 97-65

Sugihara-Seki M., Skalak R., 1988. Numerical study of asymmetric flows of red blood cells in capillaries. *Microvasc. Res.,* 36, 64-74.

Tomaiuolo G., Simeone M., Martinelli V., Rotoli B., Guido S., 2009. Red blood cell deformation in microconfined flow. *Soft Matter,* 5, 3736-3740.

Tsukada K., Sekizuka E., Oshio C., Minamitani H., 2001. Direct measurement of erythrocyte deformability in diabetes mellitus with a transparent microchannel capillary model and high-speed video camera system. *Microvasc. Res.,* 61, 231-239.

Van-Doormaal J. P., Raithby G. D., 1984. Enhancement of SIMPLE Method for Predicting Incompressible Fluid Flow. *Numer Heat Transfer,* 7, 147-163.